Telemetric Technique for Passive Resistive Sensors Based on Impedance Real Part Measurement at Fixed Frequency

Michele Bona, Michela Borghetti, Emilio Sardini, *Member, IEEE*, and Mauro Serpelloni, *Member, IEEE*

***Abstract*— This paper proposes a measurement technique for telemetric systems working with passive resistive sensors from the kilohm order. It permits calculating sensor output through analytical formulas, from system parameters and the real part of system impedance measured at readout inductor's terminals. Impedance measurement is performed always at a fixed frequency, when inductors are at a fixed relative position. Formulas were derived through specific analyses, starting from a circuit model of the system. The technique was validated by finding the output of discrete commercial resistors attached to an inductor. A difference lower than 0.98% was obtained between resistors' values calculated through the proposed technique, and their values measured by means of an impedance analyzer. Finally, we applied the technique to a real application, i.e., temperature monitoring in an enclosed environment. We used a telemetric configuration with a Pt1000 sensor to monitor the temperature inside an oven wirelessly. The results pointed out that the technique permitted to estimate the temperature with an average difference of 2.2 °C with respect to a reference. Then, uncertainty on calculated temperature was equal to ±1.2 °C. In general, work analyses highlight that measuring impedance real part may be preferred than measuring its phase angle. These achievements show the feasibility of estimating the output of a resistive sensor through the proposed technique.**

***Index Terms*— Fixed frequency, impedance real part, measurement technique, resistive sensor, telemetric system, temperature monitoring.**

I. Introduction

IN MANY applications, the characteristics of measurement environment could compromise the correct operation of a sensor containing active electronics. Examples deal with locations characterized by harsh internal conditions [1] and protected environments (e.g., human body [2]). Others regard objects that need to be kept always hermetic, such as food packages [3]. In all these cases, a passive sensor read via telemetric techniques by an external unit can be a solution.

In the literature, telemetric systems are employed in numerous applications, such as in industry [4], [5], transportation sector [6], food area [3], [7], structural health monitoring [8]–[10], and medical field [11]–[19]. Most of the works reported in the literature describe systems operating with sensors of capacitive [3]–[7], [9], [10], [12]–[14], [16], [17], [20]–[24] or inductive [15], [25] nature. On the other side, systems with resistive sensors are far less examined [18], [19], [26]–[29]. Furthermore, the few works considering resistive sensors require the voltage measurement at three different frequency points [18], the measurement of both an impedance point and the corresponding frequency [29], or a sweep to determine system quality factor [19] or resonant frequency [26].

In this paper, a technique that permits to use a resistive sensor connected to a telemetric system is proposed. Such technique needs to perform only one measurement at a fixed frequency. Furthermore, it is suitable for systems operating with resistive sensing elements whose range starts from the kilohm order, such as thermistors and Pt1000 sensors. The corresponding approach is based on the measurement of system impedance at readout inductor's terminals. In previous works, we had proposed a telemetric technique for strain [27] and temperature [28] monitoring through a resistive sensor. This approach is based on a measurement of impedance phase angle always at the same working frequency. However, such measurement is affected by the vicinity between working frequency and the one identifying phase angle minimum, which is a condition assuring a satisfying sensitivity to sensor output variation. This condition depends on the distance between system inductors, as documented also by Nopper *et al*. [30]. Furthermore, the results showed that the technique implementation requires complex dedicated electronic circuits, capable of measuring phase angle with high resolution. On the other hand, the technique proposed in this paper allows calculating sensor output through analytical formulas, from system parameters and impedance real part, which is measured always at a fixed frequency. This could permit the adoption of a simpler readout electronics.

Three main parts can be identified in this paper. Section II describes a circuit model representing the telemetric system. Then, it illustrates the analytical expressions that were derived from this model to calculate sensor output and presents the measurement technique. Section III describes how the proposed technique was experimentally validated by finding the output of commercial discrete resistors. Section IV shows the technique application to a real task, i.e., temperature

Manuscript received November 11, 2017; revised February 9, 2018; accepted February 17, 2018. Date of publication March 15, 2018; date of current version August 9, 2018. The Associate Editor coordinating the review process was Dr. Vedran Bilas. *(Corresponding author: Michele Bona.)*

The authors are with the Department of Information Engineering, University of Brescia, 25123 Brescia, Italy (e-mail: m.bona002@unibs.it).

Color versions of one or more of the figures in this paper are available online at http://ieeexplore.ieee.org.

Digital Object Identifier 10.1109/TIM.2018.2811279

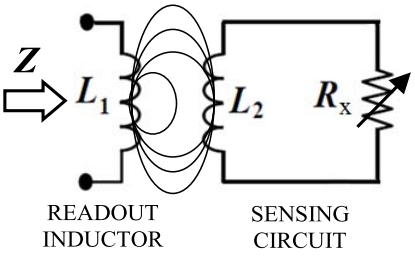

Fig. 1. Circuit representation of a telemetric system operating with a resistive sensor.

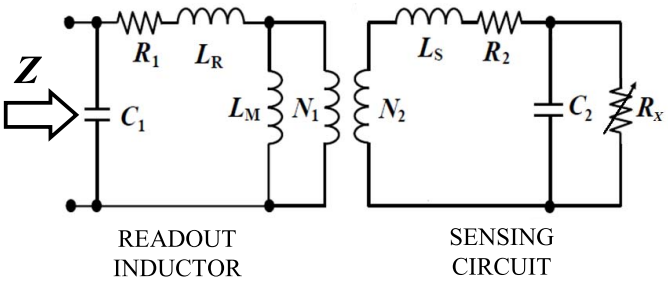

Fig. 2. System circuit model considering inductors' parasitic elements.

monitoring in an enclosed environment. In Sections III and IV, experimental analyses on physical setups together with achieved results are reported.

II. Telemetric Measurement Technique

A. System Model

A telemetric system connected with a passive resistive sensor can be generalized with the circuit model reported in Fig. 1. This general model is composed of a resistive sensor (R_x) and two coupled inductors (L_1 and L_2). R_x represents sensor resistance, which changes according to the variation of the quantity of interest measured by the sensor. Its range starts from the kilohm order. Then, the inductor connected to the sensor is called "sensing inductor" and L_2 is its self-inductance. It composes a "sensing circuit" with resistive sensor. Finally, the inductor connected to readout unit is called "readout inductor" and L_1 is its self-inductance. During system operation, impedance Z is measured at readout inductor's terminals.

Starting from the model reported in Fig. 1, in this paper we propose a more complete model including inductors' parasitic elements (Fig. 2). In Fig. 2, N_1 and N_2 are the equivalent number of windings related to L_1 and L_2, respectively. C_1 and C_2 are inductors' parasitic capacitances, whereas R_1 and R_2 are their parasitic resistances. In addition, inductances L_R and L_S represent leakage fluxes from readout and sensing inductors, respectively. On the other hand, inductance L_M models the coupling flux between the inductors [31]–[33]. Parameters

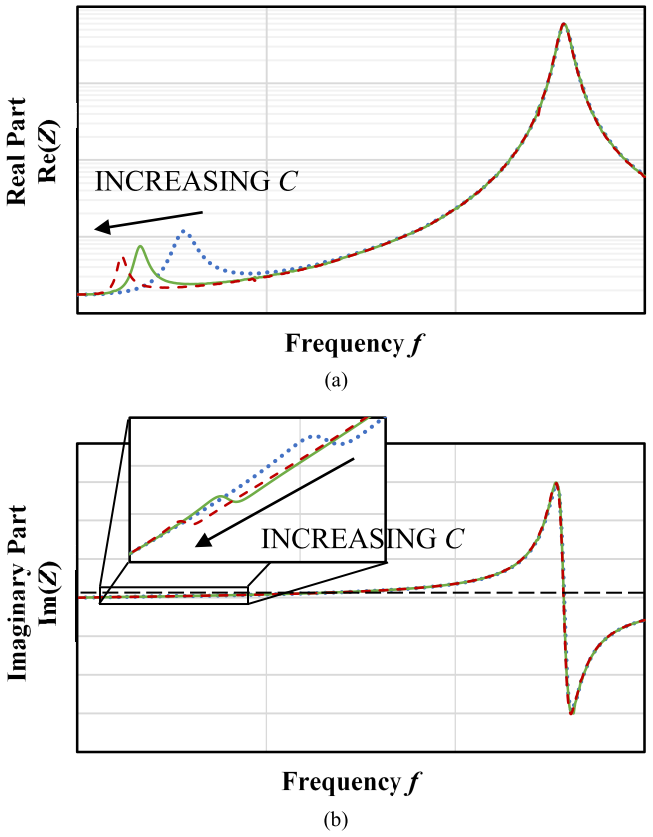

Fig. 3. Qualitative curves of impedance Z at readout inductor's terminals as a function of frequency f, for increasing values of capacitance C. (a) Real part Re(Z). (b) Imaginary part Im(Z).

L_R, L_S, and L_M are influenced by the relative position between the inductors. They depend on L_1 and L_2 through (1) and (2) [33], where the windings ratio n is equal to N_1/N_2

$$L_1 = L_M + L_R \tag{1}$$

$$L_2 = L_S + L_M/n^2. \tag{2}$$

The common qualitative impedance behavior of a telemetric system is shown as real part Re(Z) in Fig. 3(a) and imaginary part Im(Z) in Fig. 3(b). These curves can be obtained from either software simulations or experimental tests on a real telemetric system. As a first approximation, the position of each peak can be regulated independently of the other one, by acting on C_1 and C_2. For example, C_1 regulates the higher frequency peak, whereas C_2 adjusts the lower frequency one. In our telemetric technique, we propose to add a capacitor C in parallel to the high-value resistive sensor, in order to control peaks relative position. In this regard, Fig. 3 reports typical graphs of Z when C changes. It shows that C increase causes a

$$Z(j2\pi f) = \frac{R_1(R_2+R_x)-4\pi^2[L_2(L_1-\beta)+R_xC(L_1R_2+L_2R_1)]f^2+j[2\pi(L_1R_2+L_1R_x+L_2R_1+R_xCR_2R_1)f-8\pi^3R_xCL_2(L_1-\beta)f^3]}{(R_2+R_x)-4\pi^2R_xCL_2f^2+j2\pi(L_2+R_xCR_2)f} \tag{3}$$

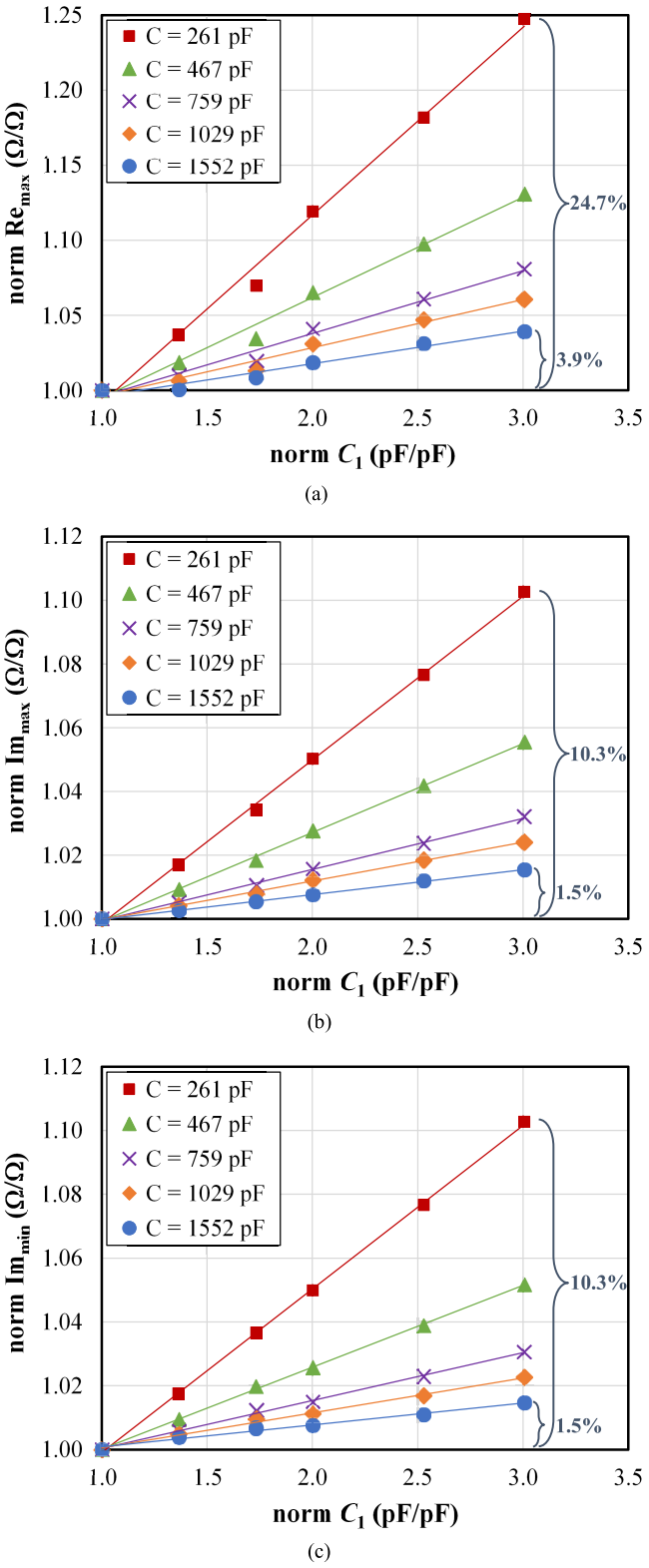

Fig. 4. Normalized values of Z lower frequency peaks as a function of normalized capacitance C_1, for different values of capacitance C. (a) Real part relative maximum Re_{max}. (b) Imaginary part relative maximum Im_{max}. (c) Imaginary part relative minimum Im_{min}.

shift of lower frequency peak toward arrow direction, whereas the higher frequency peak remains still. Therefore, there is a large distance between the frequencies of the two peaks.

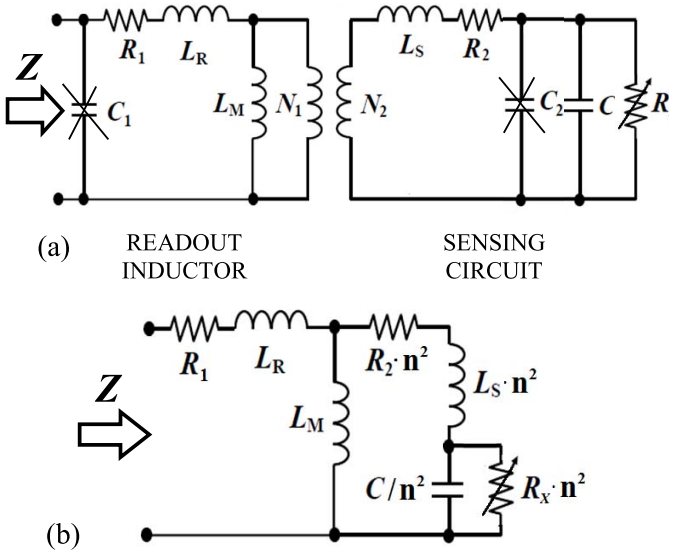

Fig. 5. (a) System model simplifications. (b) Simplified model, with sensing circuit elements seen as reflected load with respect to readout inductor.

Moreover, if such distance augments, then C_1 influence on lower frequency peak decreases, even if its value changes. This is highlighted by Fig. 4, which results from a study evaluating the variation of $\mathrm{Re}(Z)$ and $\mathrm{Im}(Z)$ lower frequency peaks consequent to C_1 and C change. In particular, Fig. 4(a)–(c) represents real part relative maximum Re_{max}, imaginary part relative maximum Im_{max}, and imaginary part relative minimum Im_{min}, respectively, as a function of C_1, for different values of C. Peaks and C_1 are normalized with respect to their first values. In general, Fig. 4 shows how peaks variation with C_1 is greatly reduced if C increases. For instance, when C_1 triples, Re_{max} change passes from 24.7% for $C = 261$ pF to 3.9% for $C = 1552$ pF (this is highlighted in Fig. 4). In the same conditions, Im_{max} and Im_{min} variation decreases from 10.3% to 1.5%. As verified by simulation and experimental tests, if the distance between the peaks is at least a decade, then C_1 influence on lower frequency peak becomes negligible. Furthermore, C_2 value can be considered insignificant with respect to C, since C is chosen to have a greater value. However, if the distance between the peaks increases, then the amplitude of lower frequency peak decreases. Thus, we choose to adjust C value to achieve a condition in which lower frequency peak is at about one decade from higher frequency peak. This consideration permits to exploit a simpler model of the system, which neglects the parasitic capacitances.

The introduced simplifications on system model are reported in Fig. 5(a). On the other hand, Fig. 5(b) shows the resulting model, where readout inductor sees sensing circuit as a reflected load through n. Equation (3), as shown at the bottom of the previous page, is the analytical expression of Z as a function of frequency f. It was found by combining the elements of the model of Fig. 5(b). It presents parameter β, which depends on coupling inductance L_M, as seen in (4). Therefore, according to (4), β is the only term in (3) depending

TABLE I
VALUES ASSUMED BY INVOLVED PARAMETERS DURING SIMULATION STUDY

Parameter	Value (unit)	Parameter	Value (unit)
L_1	47.53 (μH)	C	564.99 (pF)
R_1	35.66 (Ω)	β	0.56 (μH)
L_2	12.21 (μH)	R_x	1498.01÷9980.41 (Ω)
R_2	9.26 (Ω)	f	1.7÷2.1 (MHz)

on the relative position between the inductors

$$\beta = \frac{L_M^2}{L_2 n^2}. \tag{4}$$

B. Definition of R_x Value as a Function of Re(Z)

According to the previous theory, the circuit model of Fig. 5(b) was applied to represent a real telemetric system (which will be described in detail in Section III). Its behavior was evaluated through simulations with MATLAB (The MathWorks, Inc.), considering different values of R_x. The values assumed by model parameters are listed in Table I. They were chosen to be comparable with those presented in Section III. In this way, simulation study could provide results close to those achieved from the analysis on a real system.

Fig. 6 shows the curves of Re(Z) and Im(Z) as a function of frequency f, for different values of R_x. Both graphs highlight Z dependence on R_x. Then, with reference to Fig. 6(a), frequency $f_{\max}$ at which Re(Z) reaches its maximum slightly changes. In fact, its percentage deviation with respect to its initial value (i.e., $f_{\max,0}$ at $R_x = 1498.01\Omega$) is less than 0.4%. On the other side, as seen also in Fig. 6(b), Im(Z) peak frequencies are more variable with R_x. In fact, their percentage deviation doubles if compared to the one regarding $f_{\max}$. In addition, a deeper analysis points out that $f_{\max}$ is very close to frequency f_w, along R_x range. Frequency f_w is defined as

$$f_w = \frac{1}{2\pi\sqrt{L_2 C}}. \tag{5}$$

In fact, simulation study permitted to estimate a difference between these two frequencies smaller than 0.3%. Such difference is the same when simulating to put the inductors at any distance, by modifying the value of parameter β. Consequently, Re(Z) is a function even more suitable than phase angle, for our analysis. As a first approximation, we considered either $f_{\max}$ as still, or f_w and $f_{\max}$ as equivalent. Probably, measuring impedance magnitude $|Z|$ would be simpler than measuring Re(Z). However, $|Z|$ does not coincide with Re(Z), as Im(Z) at f_w is not null, as seen in Fig. 6(b).

Equation (6), as shown at the bottom of this page, is the analytical expression of Re(Z), which was derived from (3).

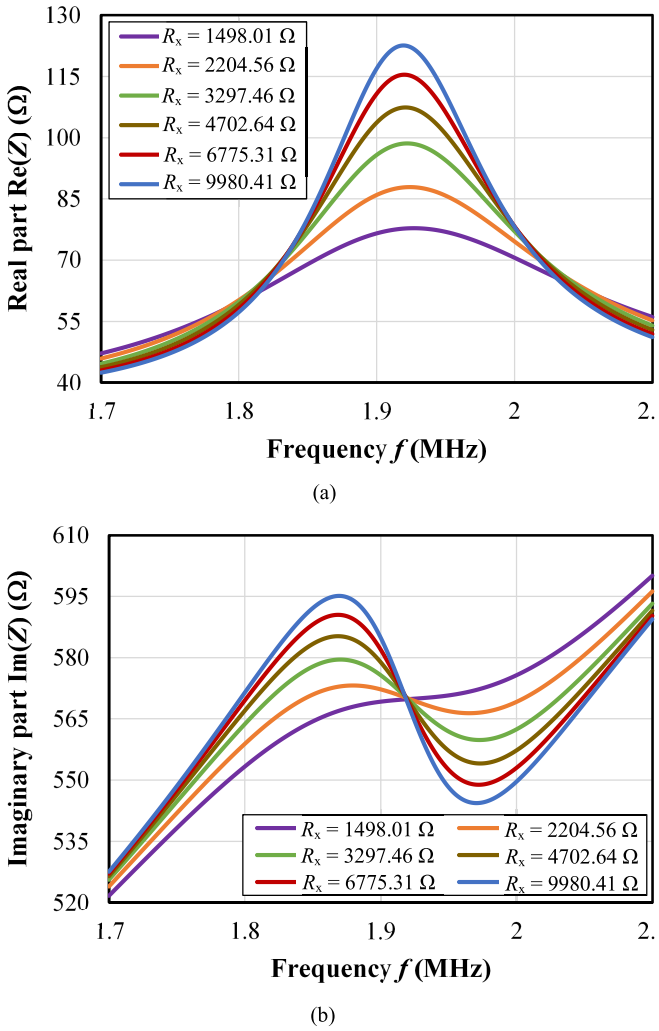

Fig. 6. Curves of impedance Z at readout inductor's terminals as a function of frequency f. They were obtained by changing the value of R_x during simulation study. (a) Real part Re(Z). (b) Imaginary part Im(Z).

As anticipated in Section I, the proposed technique is suitable for resistive sensors whose output starts from the kilohm order. Therefore, R_x is much greater than R_2 (which is usually in the order of some ohms or tens of ohms). Consequently, the following approximation can be accepted:

$$R_2 + R_x \cong R_x. \tag{7}$$

Taking into account (5) and (7), (6) becomes

$$\mathrm{Re}_w = Re(Z(f_w)) = \frac{\beta R_x}{L_2 + R_x C R_2} + R_1. \tag{8}$$

Working at f_w leads to an important simplification of (6) into (8). Finally, terms of (8) are reordered to isolate R_x

$$R_x = \frac{L_2(\mathrm{Re}_w - R_1)}{\beta - C R_2(\mathrm{Re}_w - R_1)}. \tag{9}$$

$$\mathrm{Re}(Z(f)) = \frac{R_1(R_2+R_x)^2+4\pi^2 L_2(R_2+R_x)(\beta-2R_1R_xC)f^2+4\pi^2R_1(L_2+R_xCR_2)^2f^2+16\pi^4L_2R_x^2C^2(\beta R_2+R_1L_2)f^4}{(R_2+R_x-4\pi^2R_xCL_2f^2)^2+4\pi^2(L_2+R_xCR_2)^2f^2} \tag{6}$$

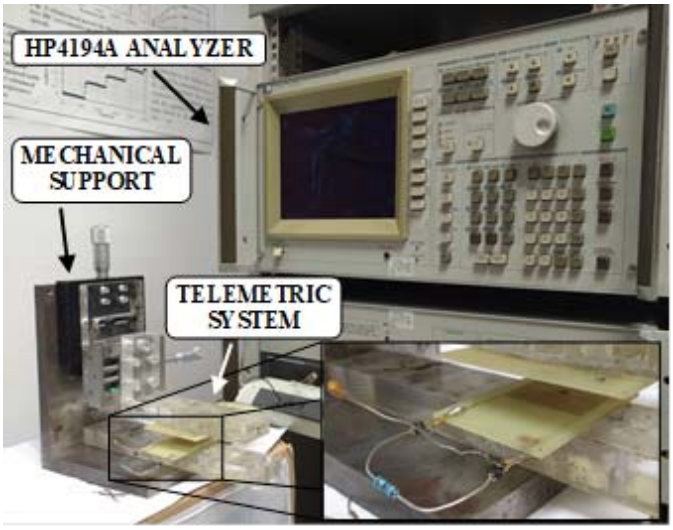

Fig. 7. Experimental setup used for technique validation tests.

Equation (9) provides a mathematical formula for calculating R_x from Re_w measurement, which is performed at readout inductor's terminals. Such approach allows measuring, with the maximum sensitivity, just the real part of system impedance at frequency f_w. This avoids the execution of any frequency sweep. In addition, (9) is simpler than the equations obtained from [27]. Parameters L_2, R_1, and R_2 are characteristic elements of the two inductors. Then, C is a capacitance whose value is chosen in order to use the simplified model of Fig. 5(b), as explained in Section II-A. All of them are supposed to be constant. On the contrary, parameter β depends on the distance between the inductors when telemetric system is in operation, whatever resistive sensor is attached. When such distance is fixed, β does not change and can be experimentally found by measuring Re_w in correspondence of one known value of R_x. In this case, it is equal to

$$\beta = \frac{L_2(\mathrm{Re}_{w,0} - R_1)}{R_{x,0}} + C R_2(\mathrm{Re}_{w,0} - R_1) \qquad (10)$$

$R_{x,0}$ is sensor resistance at the considered known condition, whereas $\mathrm{Re}_{w,0}$ is the corresponding measured impedance point at f_w. Equation (10) has been obtained by reordering (8).

III. Technique Validation: Experimental Analysis

The proposed technique was validated by using two inductors and commercial resistors that were previously characterized with an impedance analyzer HP4194A. Data and results from the present analysis report an estimation of the uncertainty referring to a 95% confidence interval (CI).

A. Experimental Setup

The dedicated laboratory setup is shown in Fig. 7. The telemetric system consists basically of a resistor representing the sensor, two square planar inductors, which were fabricated through printed circuit board (PCB) techniques on a substrate of FR4 glass-reinforced epoxy, and a capacitor C for setting f_w. We measured their values with HP4194A impedance analyzer. Table II reports inductors' geometric characteristics and the measured values of the elements of their equivalent circuits (called electrical characteristics). Values present two decimal digits, which were kept to properly include parameters uncertainty. Sensing inductor's electrical characteristics were obtained with C connected to inductor's terminals.

TABLE II
Inductors Characteristics

Property	Sensing inductor (unit)	Readout inductor (unit)
Geometric Characteristics		
Outer side (mm)	27	50
Inner side (mm)	5	27
Number of windings	27	28
Windings width (μm)	200	150
Windings spacing (μm)	200	250
Electrical Characteristics		
Equivalent inductance (μH)	12.21 ± 0.01	47.53 ± 0.12
Equivalent resistance (Ω)	9.26 ± 0.05	35.66 ± 0.09
Equivalent capacitance (pF)	564.99 ± 0.15	3.21 ± 0.01

TABLE III
Comparison Between R_X Values Calculated Through the Proposed Technique and the Measured Values of Each Resistor

MEASURED R_x	CALCULATED R_x	% DIFFERENCE
1196.89 ± 2.30	1196.89 ± 12.74	0.00 ± 1.08
1498.01 ± 2.88	1497.06 ± 16.75	0.06 ± 1.13
1789.53 ± 3.44	1780.47 ± 20.88	0.51 ± 1.18
2204.56 ± 4.24	2199.46 ± 27.94	0.23 ± 1.28
2696.29 ± 5.19	2689.97 ± 38.07	0.23 ± 1.43
3297.46 ± 6.34	3283.77 ± 50.13	0.42 ± 1.53
3906.42 ± 7.51	3891.81 ± 65.59	0.37 ± 1.69
4702.64 ± 9.05	4672.52 ± 86.28	0.64 ± 1.85
5603.41 ± 10.78	5574.35 ± 115.82	0.52 ± 2.08
6775.31 ± 13.03	6734.35 ± 159.17	0.60 ± 2.36
8178.34 ± 15.73	8111.78 ± 219.83	0.81 ± 2.70
9980.41 ± 19.20	9882.31 ± 312.46	0.98 ± 3.14

Left column of Table III lists the measured values of used commercial resistors, which we considered as pure resistances around f_w, as confirmed by the study on their impedance with HP4194A analyzer. A mechanical support keeps the inductors parallel and coaxial, at a relative distance of 20 mm (controlled through micrometric screws). A virtual instrument (VI) written with LabVIEW (National Instruments) ran on a laptop (it is not shown in Fig. 7), interfacing to HP4194A analyzer through a GPIB-USB high-speed module, in order to acquire Z.

B. Measurement Protocol

In the preliminary stage, the value of parameter β for the employed setup was obtained. We used the first resistor in

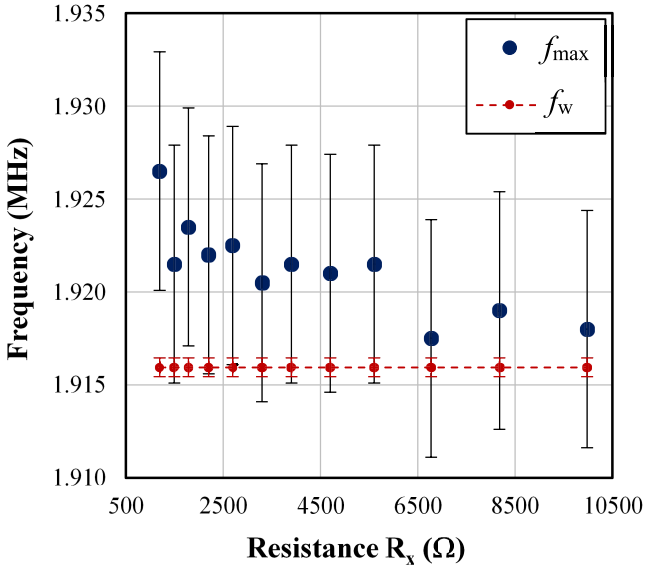

Fig. 8. Frequencies $f_{\max}$ and f_w as a function of R_x.

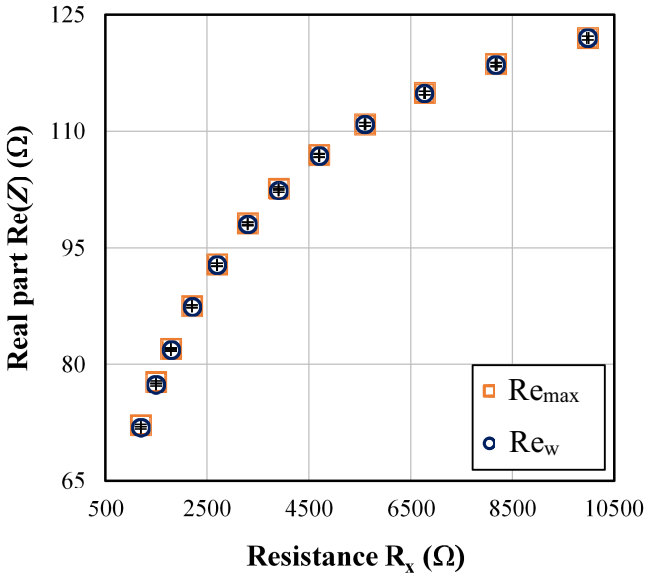

Fig. 9. Points $\mathrm{Re}_{\max}$ and Re_w as a function of R_x. Uncertainty on R_x is the one reported in the left column of Table III. Average uncertainty on $\mathrm{Re}_{\max}$ and Re_w is ± 0.19 and ± 0.20 Ω, respectively.

the left column of Table III as $R_{x,0}$ and we measured $\mathrm{Re}_{w,0}$ by means of HP4194A analyzer. Finally, we obtained $\beta = 0.558 \pm 0.003$ μH from (10). Related uncertainty was derived by applying the propagation rules to (10).

In the following stage, the proposed technique for R_x estimation was applied. The 1498.01 ± 2.88 Ω resistor was attached to the system. Then, the VI acquired the corresponding value of Re_w from HP4194A analyzer and it calculated R_x value by implementing (9). Such operation was repeated for all the resistors listed in the left column of Table III.

C. Experimental Results

Fig. 8 compares measured frequency $f_{\max}$ with f_w, which was calculated through (5), as a function of R_x. Vertical bars refer to the uncertainty on $f_{\max}$ measurement due to HP4194A analyzer uncertainty. Frequency f_w is equal to 1.916 MHz ± 800 Hz. Uncertainty on f_w was obtained by applying the propagation rules to (5). The mean difference between f_w and $f_{\max}$ was lower than 0.6%, confirming simulation results of Section II-B.

Fig. 9 shows the measured values of Re_w and $\mathrm{Re}_{\max}$ as a function of R_x. The bars related to the uncertainty on Re_w, $\mathrm{Re}_{\max}$, and R_x are present, but they are barely visible. The former takes into account both HP4194A analyzer accuracy in Re_w measurement and system capability to identify the right value of f_w. In fact, uncertainty on f_w is reflected also in the corresponding amplitude point. Uncertainty on Re_w is equal to ± 0.20 Ω, considering the mean along R_x range. On the other side, uncertainty on R_x is the one reported in the left column of Table III. Fig. 9 points out how Re_w total variation is close to 70% with respect to its first value. However, it is not uniform along R_x range. Consequently, system sensitivity to R_x change is not constant, but it is comparable with the best case, which is achieved by measuring $\mathrm{Re}_{\max}$. In fact, from the data reported in Fig. 9, we estimated a 0.48% maximum difference between Re_w and $\mathrm{Re}_{\max}$ (vicinity between $f_{\max}$ and f_w is reflected also on the corresponding real part points). Then, uncertainty on $\mathrm{Re}_{\max}$ is ± 0.19 Ω on average. It was estimated from HP4194A analyzer accuracy in measuring such point. On the other side, we measured also phase angle (as done in [27] and [28]) with used setup. For the same R_x values as those considered in Table III, phase angle presents a 6% total decrease with respect to its first value. Therefore, the real part has a greater variation than that characterizing phase angle, for identical R_x changes.

Finally, the central column of Table III reports R_x values calculated through the proposed technique, in order to obtain a more effective comparison with measured values. Associated uncertainty varies between ± 12.74 and ± 312.46 Ω. It was estimated by applying the propagation rules to (9). It is always greater than the uncertainty on measured R_x, since it takes into account the contributions provided by all the parameters present in (9). Anyway, it is at most 3% of the corresponding average. Furthermore, mean difference between calculated and measured values goes from 0.06% to 0.98%, as reported in the right column of Table III. Such difference increases to about 4% in the worst case, considering the uncertainty. In general, results from this analysis demonstrate that $\mathrm{Re}(Z)$ is a suitable function to exploit and that the proposed technique is effective in estimating the output of a passive resistive sensor.

IV. Application to Temperature Monitoring

Although it is valid for telemetric systems working with any resistive sensor from the kilohm order, we applied the technique for a specific real application. In this section, we describe how we monitored the temperature in an oven. In fact, this is one of the most required tasks in many fields, since it is critical for controlling numerous processes. As in Section III, data and results include the uncertainty for a 95% CI.

A. Experimental Setup

We used a telemetric system with two PCB planar inductors. Table IV reports their geometric and electrical characteristics.

TABLE IV
INDUCTOR CHARACTERISTICS

Property	Sensing inductor (unit)	Readout inductor (unit)
Geometric Characteristics		
Outer side (mm)	27	50
Inner side (mm)	4	27
Number of windings	23	28
Windings width (μm)	300	150
Windings spacing (μm)	200	250
Electrical Characteristics		
Equivalent inductance (μH)	7.05 ± 0.01	47.53 ± 0.12
Equivalent resistance (Ω)	1.899 ± 0.004	35.66 ± 0.09
Equivalent capacitance (pF)	564.99 ± 0.15	3.21 ± 0.01

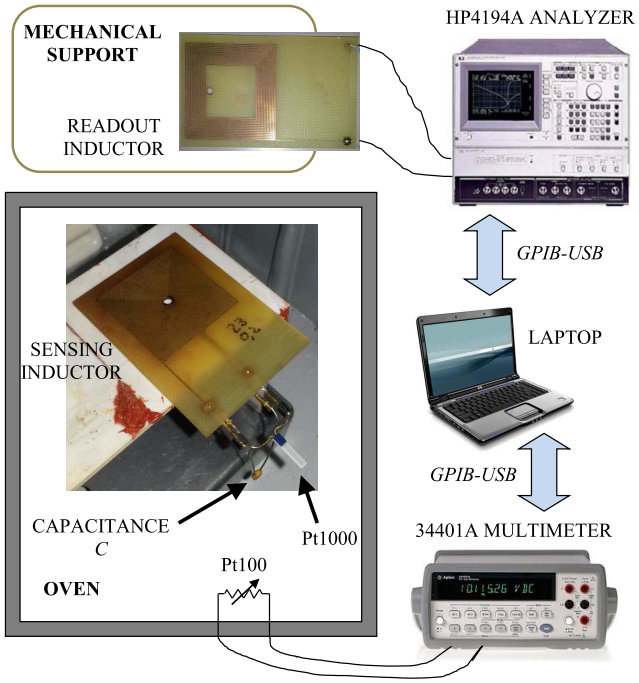

Fig. 10. Schematic of the experimental setup used for temperature monitoring.

(The latter were measured with HP4194A analyzer.) Sensing inductor's electrical characteristics consider the addition of a capacitor C. Thus, f_w is close to 2.52 MHz, as derived from (5).

Fig. 10 shows the schematic of the used experimental setup. We attached a Pt1000 resistive temperature sensor (Class A, according to standard EN 60751) in parallel to sensing inductor and capacitor C. These elements compose system's sensing circuit, which was positioned in the oven. Because of its output range, Pt1000 sensor is suitable for technique implementation. We positioned a second temperature sensor (Class A Pt100), which had been already fixed to the oven as reference sensor, close to Pt1000, at a relative distance of few centimeters. In this way, measurement discrepancies due to temperature heterogeneity inside the oven could be neglected. Then, after

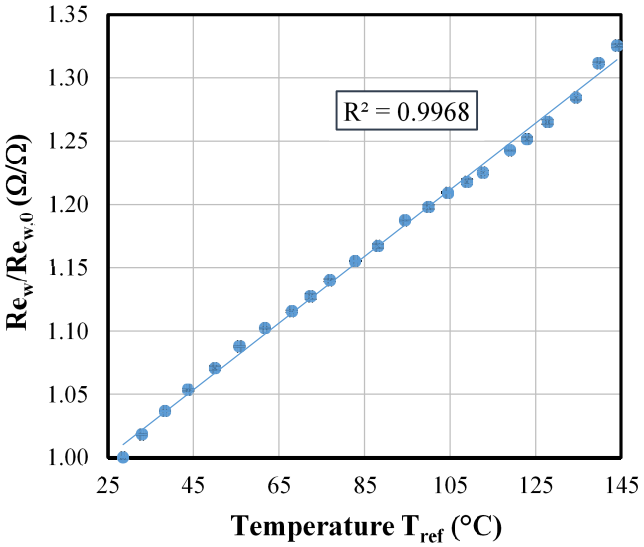

Fig. 11. Normalized Re_w as a function of reference temperature T_{ref}.

having closed the oven, we put readout inductor in parallel and coaxial position with respect to sensing inductor, at a distance of 20 mm, outside the oven. Readout inductor's terminals were connected to HP4194A analyzer, while Pt100 was attached to an Agilent 34401A digital multimeter. Both instruments were interfaced to a laptop through GPIB-USB high-speed modules. A VI was executed on laptop to guarantee synchronous data acquisition from HP4194A analyzer and 34401A multimeter and for implementing technique mathematical formulas.

B. Measurement Protocol

The first step was the calculation of parameter β for the used setup. While oven was at room temperature (which is the known condition), the VI running on laptop drove HP4194A to measure $\mathrm{Re}_{w,0}$. Then, β was calculated by implementing (10).

At this point, the system was ready to work continuously. Oven temperature was increased from about 27 °C to about 145 °C, by successive step inputs of about 5 °C. This range permits us to evaluate how the technique works in a real case. Furthermore, it allows a proper comparison with the results reported in [28]. After each step, the achieved condition has been maintained for three minutes. In this way, temperature around sensors could be considered as homogenous and stabilized. At the same time, analyzer and laptop measured Re_w and calculated R_x by applying (9). Finally, each value of R_x was converted into temperature, by considering Pt1000 linear relationship [34]. In a similar way, after measuring Pt100 resistance, we applied the corresponding relationship [34] to estimate reference temperature.

C. Experimental Results

Fig. 11 represents the variation of point Re_w consequent to temperature increase. In particular, Re_w is normalized to its value $\mathrm{Re}_{w,0}$ assumed at the beginning of the test. Fig. 11 shows a linear relationship between Re_w and temperature T_{ref}, within the range considered in the analysis. In fact, a straight line

approximates this series with a coefficient of determination R^2 close to 0.997. Furthermore, such graph highlights that Re_w has a total increase greater than 30%. In similar conditions, [28] reports that measured point of impedance phase angle decreases of less than 3%, which is a much smaller variation if compared to real part. This confirms the results illustrated in Section III. Given phase angle sensitivity to temperature variation [28], this means that a readout system needs to measure it with a resolution of two decimal digits, at least. On the other side, Re_w measurement can be performed more easily by a simpler readout circuit to obtain the same results. For these reasons, $\mathrm{Re}(Z)$ may be preferred to phase angle measurement. In addition, average uncertainty on Re_w is $\pm 0.10\ \Omega$, whereas average temperature uncertainty along the considered range is ± 0.4 °C. The latter was estimated by applying the propagation rules to Pt100 linear relationship, and taking into account both sensor and multimeter measurement accuracies.

Finally, for what concerns temperature values calculated through the proposed technique, their difference with respect to reference values is between 0.1 °C and 4.9 °C. It is 2.2 °C on average along the considered temperature range. Furthermore, uncertainty on calculated temperature is ± 1.2 °C, on average. It was derived by applying the propagation rules to Pt1000 linear relationship, starting from the uncertainty due to technique implementation (Section III) and sensor accuracy. In general, these results are comparable with those achieved starting from phase angle measurement [28]. In addition, they provide a better uncertainty on temperature estimation than the technique relying on resonant frequency determination [26]. Furthermore, the best achievements are similar to those obtained through the approach based on quality factor calculation [19]. Anyway, results suggest that the proposed technique offers a satisfying temperature estimation, considering also the examined temperature range. In fact, even the worst result can be acceptable in applications where temperature range is close to 100 °C [26]. Then, it has the advantage to work at a fixed frequency, with respect to other approaches [19], [26] and also to methods that exploit telemetric systems with capacitive or inductive sensors.

V. Conclusion

This paper has proposed a measurement technique for telemetric systems operating with resistive sensors from the order of the kilohm. Such technique consists in calculating sensor output through mathematical formulas, which are simpler than those found in previous works. Furthermore, it is based on a measurement of impedance real part at readout inductor's terminals at only one frequency, when system inductors are at a fixed relative position. We have explained how we validated the technique by using commercial discrete resistors (from about 1000 to about 10 000 Ω) and a custom setup. Then, we have reported the obtained results, with respect to a reference. Furthermore, we have applied the proposed technique to a common task, i.e., temperature monitoring in an oven. As for technique validation tests, we have presented both the used the laboratory setup and the experimental results.

In general, such achievements highlight the effectiveness of our solution, which has the advantage of working at a fixed frequency. In addition, performed analyses have pointed out that measuring real part may be better than measuring phase angle. Therefore, the proposed technique is a valid option when a telemetric system has to be employed, or when a resistive sensor is preferred to a capacitive or inductive one.

Future work will involve further studies to assess technique accuracy and precision, by taking into account wider temperature ranges and different kinds of resistive sensor, e.g., strain sensors, as done in [27]. By the way, there are some possibilities to consider for extending technique application. For instance, addressing the limitation to keep the inductors at a fixed position would permit to obtain results not dependent on its variation, as achieved in [31] for telemetric systems working with a capacitive sensor.

References

[1] T. George, K.-A. Son, R. A. Powers, L. Y. Del Castillo, and R. Okojie, "Harsh environment microtechnologies for NASA and terrestrial applications," in *Proc. IEEE Sensors*, Irvine, CA, USA, Oct./Nov. 2005, pp. 1253–1258.

[2] G. S. Wilson and R. Gifford, "Biosensors for real-time *in vivo* measurements," *Biosensors Bioelectron.*, vol. 20, no. 12, pp. 2388–2403, Jun. 2005.

[3] E. L. Tan, W. N. Ng, R. Y. Shao, B. D. Pereles, and K. G. Ong, "A wireless, passive sensor for quantifying packaged food quality," *Sensors*, vol. 7, pp. 1747–1756, Sep. 2007.

[4] E. Sardini and M. Serpelloni, "Wireless measurement electronics for passive temperature sensor," *IEEE Trans. Instrum. Meas.*, vol. 61, no. 9, pp. 2354–2361, Sep. 2012.

[5] M. A. Fonseca, J. M. English, M. von Arx, and M. G. Allen, "Wireless micromachined ceramic pressure sensor for high-temperature applications," *J. Microelectromech. Syst.*, vol. 11, no. 4, pp. 337–343, Aug. 2002.

[6] M. Nabipoor and B. Y. Majlis, "A new passive telemetry LC pressure and temperature sensor optimized for TPMS," *J. Phys., Conf. Ser.*, vol. 34, no. 1, pp. 770–775, 2006.

[7] D. Marioli, E. Sardini, and M. Serpelloni, "An inductive telemetric measurement system for humidity sensing," *Meas. Sci. Technol.*, vol. 19, no. 11, pp. 115204-1–115204-8, 2008.

[8] A. Deivasigamani, A. Daliri, C. H. Wang, and S. John, "A review of passive wireless sensors for structural health monitoring," *Modern Appl. Sci.*, vol. 7, no. 2, pp. 57–76, 2013.

[9] K. Perveen, G. E. Bridges, S. Bhadra, and D. J. Thomson, "Corrosion potential sensor for remote monitoring of civil structure based on printed circuit board sensor," *IEEE Trans. Instrum. Meas.*, vol. 63, no. 10, pp. 2422–2431, Oct. 2014.

[10] G. Stojanović, M. Radovanović, M. Malešev, and V. Radonjanin, "Monitoring of water content in building materials using a wireless passive sensor," *Sensors*, vol. 10, pp. 4270–4280, Apr. 2010.

[11] W. Mokwa, "Medical implants based on microsystems," *Meas. Sci. Technol.*, vol. 18, no. 5, pp. R47–R57, 2007.

[12] M. A. Fonseca, M. G. Allen, J. Kroh, and J. White, "Flexible wireless passive pressure sensors for biomedical applications," in *Proc. Solid-State Sens., Actuators, Microsyst. Workshop*, Hilton Head Island, SC, USA, Jun. 2006, pp. 37–42.

[13] P.-J. Chen, S. Saati, R. Varma, M. S. Humayun, and Y.-C. Tai, "Wireless intraocular pressure sensing using microfabricated minimally invasive flexible-coiled LC sensor implant," *J. Microelectromech. Syst.*, vol. 19, no. 4, pp. 721–734, Aug. 2010.

[14] S. Lizón-Martínez, R. Giannetti, J. L. Rodríguez-Marrero, and B. Tellini, "Design of a system for continuous intraocular pressure monitoring," *IEEE Trans. Instrum. Meas.*, vol. 54, no. 4, pp. 1534–1540, Aug. 2005.

[15] G.-Z. Chen, I.-S. Chan, L. K. K. Leung, and D. C. C. Lam, "Soft wearable contact lens sensor for continuous intraocular pressure monitoring," *Med. Eng. Phys.*, vol. 36, no. 9, pp. 1134–1139, Sep. 2014.

[16] J. Riistama, E. Aittokallio, J. Verho, and J. Lekkala, "Totally passive wireless biopotential measurement sensor by utilizing inductively coupled resonance circuits," *Sens. Actuators A, Phys.*, vol. 157, no. 2, pp. 313–321, 2010.

[17] T. Salpavaara, J. Verho, P. Kumpulainen, and J. Lekkala, "Wireless interrogation techniques for sensors utilizing inductively coupled resonance circuits," *Procedia Eng.*, vol. 5, pp. 216–219, 2010.
[18] S. F. Pichorim and P. J. Abatti, "A novel method to read remotely resonant passive sensors in biotelemetric systems," *IEEE Sensors J.*, vol. 8, no. 1, pp. 6–11, Jan. 2008.
[19] S. S. Karipott, P. M. Veetil, B. D. Nelson, R. E. Guldberg, and K. G. Ong, "An embedded wireless temperature sensor for orthopedic implants," *IEEE Sensors J.*, vol. 18, no. 3, pp. 1265–1272, Feb. 2018.
[20] G. J. Radosavljevic, L. D. Zivanov, W. Smetana, A. M. Maric, M. Unger, and L. F. Nad, "A wireless embedded resonant pressure sensor fabricated in the standard LTCC technology," *IEEE Sensors J.*, vol. 9, no. 12, pp. 1956–1962, Dec. 2009.
[21] H. Zhang *et al.*, "Phase interrogation used for a wireless passive pressure sensor in an 800 °C high-temperature environment," *Sensors*, vol. 15, no. 2, pp. 2548–2564, 2015.
[22] C. Li *et al.*, "A noncontact wireless passive radio frequency (RF) resonant pressure sensor with optimized design for applications in high-temperature environments," *Meas. Sci. Technol.*, vol. 25, no. 7, p. 075101, 2014.
[23] Q. Tan *et al.*, "A harsh environment-oriented wireless passive temperature sensor realized by LTCC technology," *Sensors*, vol. 14, no. 3, pp. 4154–4166, 2014.
[24] C. Zhang, L.-F. Wang, J.-Q. Huang, and Q.-A. Huang, "An LC-type passive wireless humidity sensor system with portable telemetry unit," *J. Microelectromech. Syst.*, vol. 24, no. 3, pp. 575–581, Jun. 2015.
[25] J. C. Butler, A. J. Vigliotti, F. W. Verdi, and S. M. Walsh, "Wireless, passive, resonant-circuit, inductively coupled, inductive strain sensor," *Sens. Actuators A, Phys.*, vol. 102, nos. 1–2, pp. 61–66, Dec. 2002.
[26] M. Lee, K. Morimoto, and Y. Suzuki, "Flexible wireless wall temperature sensor for unsteady thermal field," *J. Phys., Conf. Ser.*, vol. 660, no. 1, pp. 012019-1–012019-5, 2015.
[27] M. Bona, M. Serpelloni, E. Sardini, C. O. Lombardo, and B. Andò, "Telemetric technique for wireless strain measurement from an inkjet-printed resistive sensor," *IEEE Trans. Instrum. Meas.*, vol. 66, no. 4, pp. 583–591, Apr. 2017.
[28] M. Bona, M. Borghetti, E. Sardini, and M. Serpelloni, "Novel telemetric technique for passive resistive sensors based on impedance phase angle measurement at constant frequency," in *Proc. IEEE I2MTC*, Turin, Italy, May 2017, pp. 1023–1028.
[29] M. Bona, E. Sardini, and M. Serpelloni, "Telemetric model for passive resistive sensors in biomedical applications," *Procedia Eng.*, vol. 87, pp. 444–447, 2014.
[30] R. Nopper, R. Niekrawietz, and L. Reindl, "Wireless readout of passive LC sensors," *IEEE Trans. Instrum. Meas.*, vol. 59, no. 9, pp. 2450–2457, Sep. 2010.
[31] D. Marioli, E. Sardini, M. Serpelloni, and A. Taroni, "A new measurement method for capacitance transducers in a distance compensated telemetric sensor system," *Meas. Sci. Technol.*, vol. 16, no. 8, pp. 1593–1599, 2005.
[32] D. Marioli, E. Sardini, M. Serpelloni, and A. Taroni, "Contactless transmission of measurement information between sensor and conditioning electronics," *IEEE Trans. Instrum. Meas.*, vol. 57, no. 2, pp. 303–308, Feb. 2008.
[33] D. Marioli, E. Sardini, and M. Serpelloni, "Inductive telemetric measurement systems for remote sensing," in *Advances in Measurement Systems*, M. K. Sharma, Ed. Rijeka, Croatia: InTech, 2010, pp. 343–364.
[34] K. Ehinger *et al.*, *Practices for Industrial Temperature Measurements*. Ladenburg, Germany: ABB Automation Products GmbH, 2013.

Michele Bona was born in Brescia, Italy, in 1989. He received the B.S. degree in industrial automation engineering from the University of Brescia, Brescia, in 2011, the joint M.S. degree (*summa cum laude*) from the University of Brescia and the Université Pierre et Marie Curie, Paris VI, Paris, France, in 2013, and the Ph.D. degree (*summa cum laude*) in information engineering from the University of Brescia in 2017.

He is currently a Post-Doctoral Fellow with the Department of Information Engineering, University of Brescia. His current research interests include measurement systems exploiting telemetric techniques and the realization of low-cost passive components through innovative technologies.

Michela Borghetti received the M.S. degree (*summa cum laude*) in electronics engineering and the Ph.D. degree in technology for health from the University of Brescia, Brescia, Italy, in 2012 and 2016, respectively.

In 2015, she was a Visiting Ph.D. Student at the Universitat Politècnica de Catalunya, Barcelona, Spain. She was a Post-Doctoral Fellow with the Department of Information Engineering, University of Brescia, until 2017. She was involved in the design and fabrication of sensors for healthcare using low-cost technologies, and development of electronic systems for measuring and monitoring limb movements.

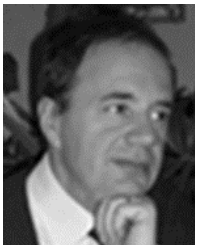

Emilio Sardini (M'99) was born in Mantua, Italy, in 1958. He received the M.S. degree in electronics engineering from the Politecnico di Milano, Milan, Italy, in 1983.

Since 1984, he has conducted research and teaching activities with the Department of Electronics for Automation, University of Brescia, Brescia, Italy, where he has been a Full Professor of electrical and electronic measurements since 2006, and the Deputy Dean of the Engineering Faculty, and is currently the Coordinator of the "Technology for Health" Ph.D. Program, the Director of the Department of Information Engineering, and a Member of the Academic Senate. He has authored or co-authored over 100 scientific papers. His current research interests include electronic instrumentation, sensors, signal conditioning electronics, and the development of autonomous sensors for biomedical applications.

Mauro Serpelloni (M'12) was born in Brescia, Italy, in 1979. He received the M.S. degree (*summa cum laude*) in industrial management engineering and the Ph.D. degree in electronic instrumentation from the University of Brescia, Brescia, in 2003 and 2007, respectively.

He was an Assistant Professor of electrical and electronic measurements with the Department of Information Engineering, University of Brescia, where he was involved in the design, modeling, and fabrication of measurement systems for industrial applications. Since 2017, he has been an Associate Professor of electrical and electronic measurements with the University of Brescia. His current research interests include biomechatronic systems, contactless transmission between sensors and electronics, contactless activation for resonant sensors, signal processing for microelectromechanical systems, and sensors fabrication through additive manufacturing technologies.